Energy materials

CrossMark

Synergetic effect of synthesized sulfonated polyaniline/ quaternized graphene and its application as a high-performance supercapacitor electrode

Shadpour Mallakpour[1,2,3,*], Amir Abdolmaleki[1,2,3,*], Manzar Mahmoudian[1], Ali A. Ensafi[1], and Mehdi Mokhtari Abarghoui[1]

[1] Department of Chemistry, Isfahan University of Technology, Isfahan 84156-83111, Iran
[2] Nanotechnology and Advanced Materials Institute, Isfahan University of Technology, Isfahan 84156-83111, Iran
[3] Department of Chemistry, Center of Excellence in Sensors and Green Chemistry, Isfahan University of Technology, Isfahan 84156-83111, Iran

ABSTRACT

A new hybrid sulfonated polyaniline/quaternized graphene (s-PANINa/q-graphene) is prepared by electrostatic and π–π interactions between positively charged quaternized graphene (q-graphene) and negatively charged sulfonated polyaniline (s-PANINa). The introduction of the s-PANINa into the q-graphene sheets leads to the formation of nanohybrid with layered morphology and high electrical conductivity. The electrochemical performance of s-PANINa/q-graphene nanohybrid as an electrode material for supercapacitors application is evaluated using cyclic voltammetry and galvanostatic charge/discharge tests in 1.0 M of H_2SO_4 as an electrolyte. The maximum capacitance of 682 F g^{-1} is obtained for s-PANINa/q-graphene nanohybrid at the current density of 1.0 A g^{-1}. 70.0% retention of the initial specific capacitance (from current density of 1.0–30 A g^{-1}), which indicates the excellent rate capability and consequently high power characteristics of s-PANINa/q-graphene nanohybrid. Moreover, the proposed nanohybrid shows an excellent stability (less than 5% drop after 2000 cycles) with about 100% of coulombic efficiency. The improved electrochemical performance because of the synergistic effects between q-graphene and the s-PANINa indicates that nanohybrid is a good candidate for high-performance supercapacitors.

Introduction

The demand for renewable energy resources and reliable energy storage devices is growing rapidly due to the limited global energy supply and environmental issues such as global warming [1]. Among all energy storage devices, electrochemical supercapacitors are attractive choice due to their outstanding cycle stability, high power density, high charge–discharge rate and

Address correspondence to E-mail: mallak@cc.iut.ac.ir; mallak777@yahoo.com; mallakpour84@alumni.ufl.edu; abdolmaleki@cc.iut.ac.ir; amirabdolmaleki@yahoo.com

Springer

low environmental impacts [2]. Energy storage in double-layer capacitors is based on non-faradic charge separations at the interface between a solid electrode and an electrolyte [3], while reversible redox reactions at/near the surface of an electrode are involved in pseudocapacitors charge storage [4]. Recent researches have been shown that the combination of both faradic and non-faradic charge storage mechanism in supercapacitors leads to the higher energy and power density as well as specific capacitance [5]. In this way, different hybrid electrode materials such as carbon cloth/MnO_2, carbon nanotubes/$NiCo_2O_4$, polypyrrole/carbon nanotubes, MoS_2/carbon aerogel, polyaniline/TiO_2 and Bi_2S_3/graphene [6–10] have been developed.

Conductive polymers, especially polyaniline, have been considered as promising pseudocapacitive materials owing to their facile synthesis, low cost, good conductivity, environmental friendliness and high specific capacitance [11]. Unfortunately, cycle stability and rate capability of conductive polymer-based supercapacitors have been hindered by swelling and shrinkage of polymer during doping and undoping process as well as and slow kinetics of charge–discharge reactions [12]. As another class of supercapacitors electrode material, graphene has attracted great interest due to its high theoretical surface area, good thermal and mechanical stability and high electrical conductivity [13]. Graphene/conductive polymer hybrids have attracted great deal of attention because they may possess novel combinations with superior electrochemical characteristics than either of the individual components [14–17]. Among them, it has been already confirmed that the hybrids consisted of polyaniline and graphene possess the superior electrochemical properties than either of the individual components, which are potential materials for the development of high-rate and stable supercapacitor electrodes [18, 19].

In this work, a new polyaniline/graphene nanohybrid has been developed for supercapacitor application. In this way (as presents in Fig. 1), q-graphene is prepared by selectively modifying quaternary ammonium in the edges and defects of graphene and PANI is synthesized and functionalized to obtain s-PANINa. Finally, to obtain some reinforcement and/or synergetic effect between polyaniline and graphene, the nanohybrid is prepared by multiple interactions (electrostatic and π–π interaction) between the layer components, including the negatively charged s-PANINa and the positively

Figure 1 Schematic diagram of the preparation procedure of the ▶ s-PANINa/q-graphene nanohybrid.

charged q-graphene. These stronger interactions avoid the restacking and aggregation of individual functionalized graphene and improve the conductivity and electrochemical performance (high-rate capability and high stability) of the nanohybrid [20].

## Experimental

Chemicals and apparatus

Graphite, $KMnO_4$, $NaNO_3$, hydrazine hydrate, iodomethane, methanol, sulfuric acid, 1,2-diaminobenzene and hydrogen peroxide were purchased from Merck Chemical Co. Aniline (99%, Aldrich) was distilled under vacuum and stored in refrigerator prior to use. Stainless steel mesh (SS), type 304 was purchased from local market.

Synthesis of GO and GO derivatives

The GO is prepared in three steps: first, the graphite is oxidized by a modified Hummers's method reveals in literatures [21]. After oxidation, the resulting graphite oxide colloid is sonicated for 1 h to acquire a GO colloid. Then, the GO powder is obtained by diluting, centrifugation and drying.

The G-BI is prepared by a reported procedure [22] and described in brief as follows: 30 mg of GO powder is dispersed in 5 mL of acetone with ultrasonication for 15 min, then 50 mg of 1,2-diaminobenzene is added to the suspension and ultrasonically treated for another hour. Subsequently, PPA (5 mL) is added under vigorous stirring, and the mixture heated at 200 °C for 15 h under nitrogen atmosphere, and the reaction mixture is poured into 200 mL of deionized water under stirring to dissolve the PPA and the GO-BI is then collected by centrifuge. The resultant GO-BI redispersed into methanol (120 mL) followed by sonication for 30 min, then hydrazine hydrate (1.4 mL) is added to the solution and refluxed at 65 °C for 24 h. After the reaction is complete, the resultant G-BI is centrifuged and washed with methanol several times. To synthesis q-graphene, 20 mg of G-BI dispersed in 100 ml of methanol, then 0.5 ml CH_3I added to the mixture and refluxed at 80 °C for 24. The product is collected by

Step 1:
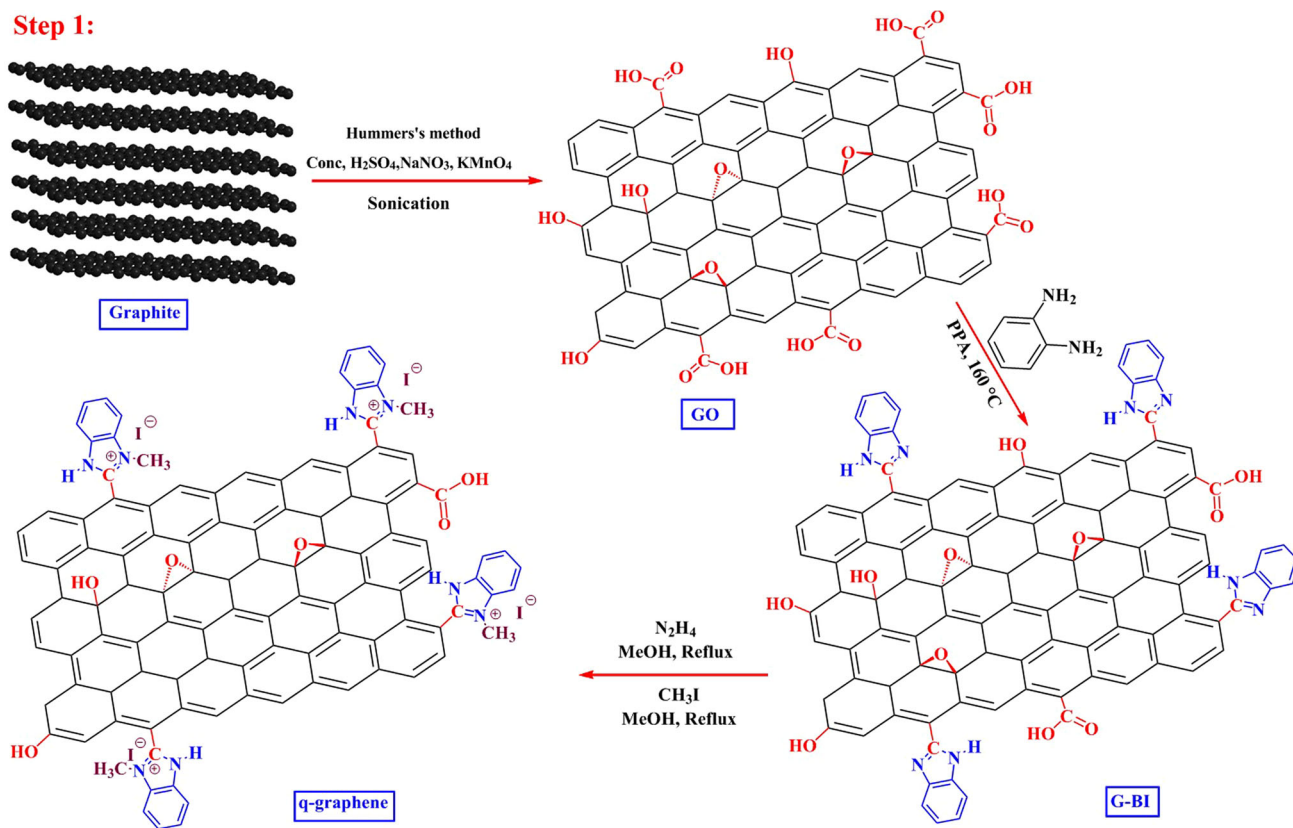
Step 2:
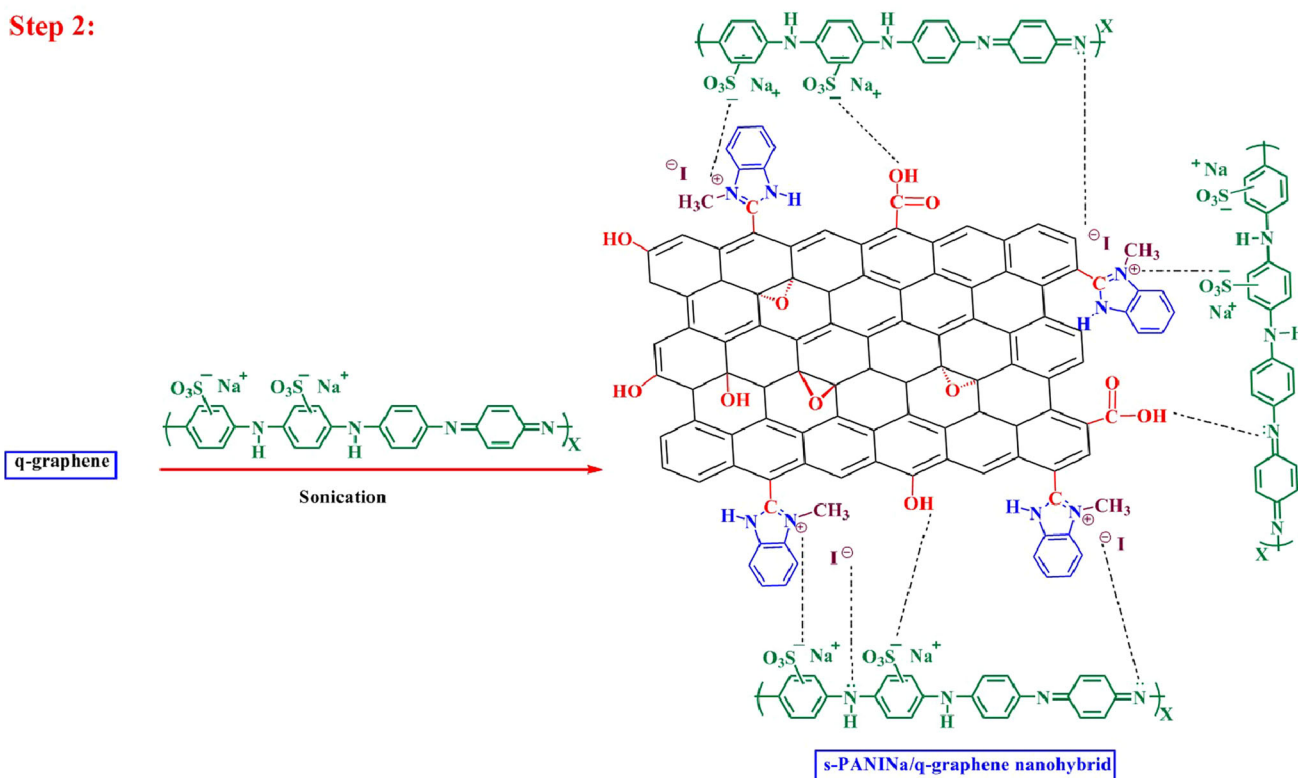
centrifuge, washed by 100 mL of methanol three times and dried under vacuum at room temperature.

Synthesis of s-PANINa and s-PANINa/q-graphene nanohybrid

The synthesis method is reported for *s-PANINa* in a previous paper [23]. Brief description of the synthesis is described as follows: PANI emeraldine base (50 mg) is sulfonated by dissolving it in 40 mL of fuming sulfuric acid and the reaction is kept stirring for 2 h at room temperature. The solution is slowly added to 300 ml mixture of methanol and acetone and also cooled to 10 °C by an ice/water bath to precipitate the product. The green powder is then collected on a Büchner funnel, washed frequently with methanol and dried under vacuum at room temperature to give dark green powder (s-PANI). The s-PANINa is synthesized by dissolving 0.25 g of s-PANI in 10 mL of 0.1 M NaOH solution and stirred for 30 min at room temperature. The dark purple powder was obtained by filtrated and repetitively washed with water.

For preparation of s-PANINa/q-graphene nanohybrid, the q-graphene (25 mg) is dispersed in 100 mL acetone with high-frequency ultrasound for 15 min to form a homogenous q-graphene suspension. Subsequently, 50 mg of *s-PANINa* is added to the suspension and ultrasonically treated for 1 h. Then, the mixture is collected by a Büchner funnel and dried in vacuum at 60 °C.

Electrode preparation

The working electrodes were fabricated by mixing of polyaniline, q-graphene or PANINa/q-graphene nanohybrid as an active material, poly(vinylidene fluoride) as a binder and carbon black as a conductive agent with weight ratio of 80:10:10 and diluted with an appropriate amount of *N*-methyl-2-pyrrolidone using ultrasonic bath to form a uniform slurry. Then, the resulting slurry were casted onto stainless steel mesh and dried in vacuum at 90 °C for 6 h to remove the solvent.

Characterization

FT-IR spectra of the as-prepared samples were recorded by a Jasco-680 (Japan) spectrometer using KBr pellets. Elemental analysis (EA) was analyzed with a CHNS-932, Leco. XRD patterns were performed using a Bruker, D8 Advanced diffractometer with a copper target at the wavelength of λ CuKα = 1.5406 Å and a tube voltage of 40 kV and tube current of 35 mA, in the range of 5–100° at the speed of 0.05 per min. Raman spectroscopy was obtained on a Almega Thermo Nicolet Dispersive Raman spectrometer by a Nd:YLF laser source operating at wavelength of 532 nm. X-ray photo-electron spectroscopy (XPS) was measured by a twin anode XR3E2 X-ray Al-based source system operating at a vacuum by X-ray 8025-BesTec spectrometer. Thermogravimetric analysis (TGA) is performed on a STA503 (Bahr-Thermoanalyse GmbH, Hüllhorst, Germany) under nitrogen atmosphere at the heating rate of 10 °C min^{-1} from 25 to 800 °C. The morphology of samples was characterized using FE-SEM (HITACHI S-4160, Japan).

Galvanostatic charge–discharge (CD) and cyclic voltammetry tests were carried out in a three-electrode cell system using an Ivium potentiostate/galvanostate instrument (pocket STAT Model) with a saturated Ag/AgCl reference electrode, a platinum counter electrode and a working electrode.

Results and discussion

Characterization of the nanohybrid

The morphologies of GO, G-BI and nanohybrid are observed with FE-SEM (Fig. 2). As shown in Fig. 2a and b, the obtained GO presents kinked and wrinkled morphology and layered structure [24]. G-BI (Fig. 2c, d) showed exfoliated morphology with many exposed edges, indicating covalent functionalization of graphene [22]. As shown in Fig. 2e, f, significant morphology changes occurred during the formation of nanohybrid. The strong electrostatic interaction between q-graphene and s-PANINa provides a confined environment and leads to the formation of nanohybrid with the mostly tubular morphology with layered structures of nanohybrid, which varied from the flake structure of G-BI [25]. Such layered structure as shown in Fig. 2e indicates that a layer of the s-PANINa surrounded by q-graphene sheets [26] and could effect to conductivity and stabilize the structure of nanohybrid during the charge–discharge process, which might lead to improve the capacitance and longer cycling life [26].

Figure 2 FE-SEM images of **a**–**b** GO; **c**–**d** G-BI [27] and **e**–**f** nanohybrid.
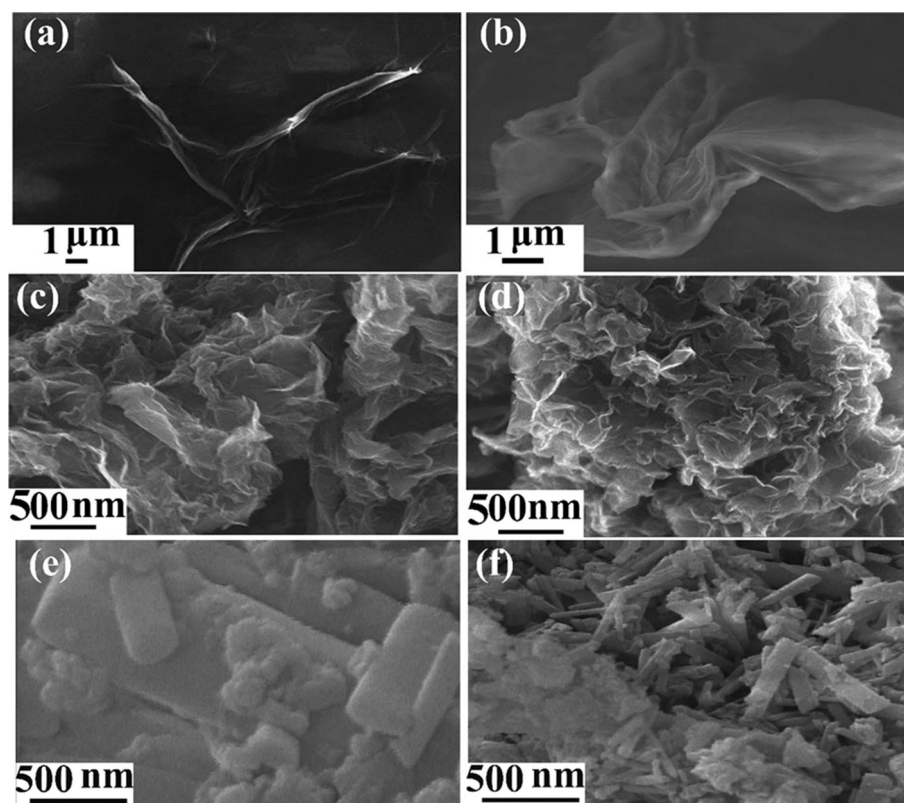
The chemical structure of the resulting G-BI, q-graphene, s-PANINa and nanohybrid further investigated by FT-IR spectroscopy (Figure S1). The spectrum of G-BI shows the characteristic adsorption peaks of C=N, and C–N stretching vibration of the benzmidazole heterocycle at the 1636, and 1416 cm^{-1}, respectively. The peak at 1563 cm^{-1} is assigned to C=C stretching of the benzene ring. The wide peak around 3400 cm^{-1} is contributed to the N–H stretch, which can be due to the overlap with reduced content of the functional groups on graphene [27]. In comparison to BI-G, the peak at 3400 cm^{-1} is disappeared in the spectrum of q-graphene; so, it is concluded that complete functionalization of the NH groups with methyl iodide. In addition, the appearance of absorption peak located at 1078 cm^{-1} demonstrates the presence of N–CH$_3$ stretching band. The FT-IR spectrum of the s-PANINa sample, the stretching vibration of the benzenoid and quinoid rings are located at 1502 and 1603 cm^{-1}, respectively. The C–N stretching band of an aromatic amine appears at 1282 cm^{-1}. Other peaks located at 1184, 1120, 849 and 606 cm^{-1} are ascribed to the -SO$_3^-$ groups [28]. In the spectrum of nanohybrid, the adsorption peak located to 1566 and 1502 cm^{-1} is assigned to the C=C

stretching of the benzene ring on the q-graphene and benzenoid rings of s-PANINa, respectively, demonstrate the presence of s-PANINa and q-graphene in the nanohybrid. Furthermore, the strong bond centered at 1128 cm^{-1} is associated to a high degree of delocalization of electrons and high conductivity of the polymer for the nanohybrid, which is also confirmed by enhanced electrical conductivity of the nanohybrid [29].
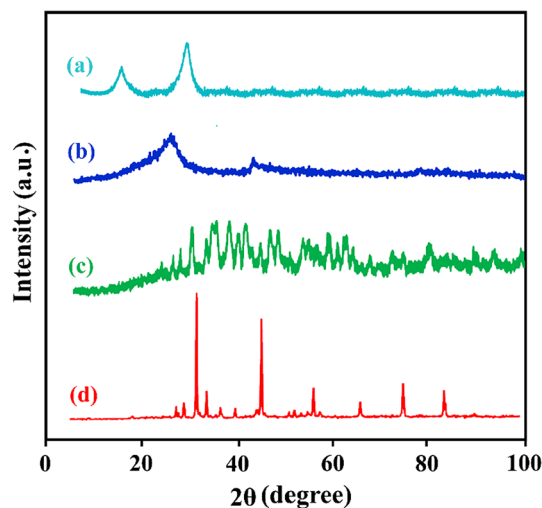
The Raman spectroscopy used as a powerful tool to investigate the interactions between graphene and s-PANINa in nanohybrid (Fig. 3). For the s-PANINa, the peak at 1596 cm^{-1} is related to the C–C stretching of the benzenoid ring and the peak at 1504 cm^{-1}, corresponding to C=N stretching of the quinonoid ring. The peak at 1339 and 1174 cm^{-1} arises from the C–N$^+$ stretching and C–H bending of the quinoid/benzenoid ring, respectively [29]. The Raman spectrum of reduced graphene oxide (rGO) exhibits two strong peaks, the G band at 1589 cm^{-1} and the D band at 1314 cm^{-1}. The G band originates from in-plane sp^2 carbon atoms, while the D band due to the sp^3 carbon atoms that originate from defects in the graphite [30]. The spectrum of nanohybrid shows two broad peaks at 1362 and 1591 cm^{-1} and the peaks of
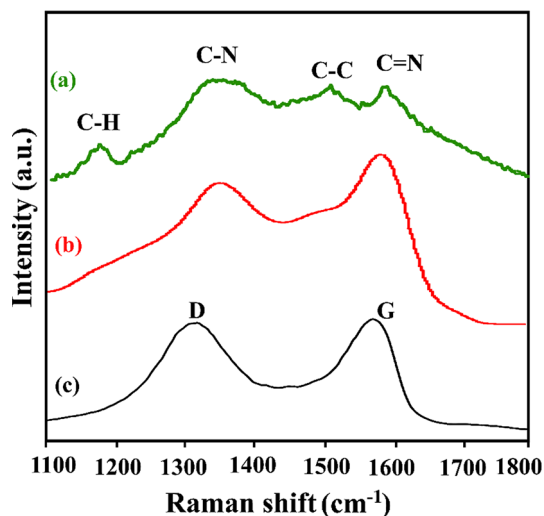
Figure 3 Raman spectra of *a* s-PANINa, *b* nanohybrid and *c* rGO.

Figure 4 XRD patterns of *a* GO-BI, *b* q-graphene, *c* s-PANINa and *d* nanohybrid.

s-PANINa apart from the D and G bands of nanohybrid that is an evidence which indicates the interaction of s-PANINa in the inner surfaces of the q-graphene sheets. Further the intensity ratio of I_D/I_G increases obviously for the nanohybrid (0.84) than pristine graphite (0.54), which demonstrates induced defects during covalent functionalization of graphene and the influence of s-PANINa on graphene due to the intimate interaction between them [21]. In addition, compared with the rGO, the D and G bands in nanohybrid exhibit blue shifts the peak at 1502 cm^{-1} shifts from 1495 cm^{-1} and the peak centered at 1476 cm^{-1} shifts from 1464 cm^{-1}. These blue shifts also approve the strong π–π interaction between the polymeric chains with the basal q-graphene sheets [31].

Thermal stabilities of G-BI, q-graphene, s-PANINa and nanohybrid are presented in Figure S2. The G-BI shows a total mass loss 12% with significant mass loss starting at about 400 °C, which is attributed to the decomposition of organic groups such as of benzimidazole groups on the graphene sheets [27]. The q-graphene sample displays gradual degradation in the region of 100–800 °C. However, the thermal stability of q-graphene considerably decreases after quaternization [32]. Compared to G-BI, the total weight loss for q-graphene is 27%, demonstrating a successful quaternization of benzimidazole groups on the graphene layers. s-PANINa sample shows weight loss below 150 °C corresponds to the removal of adsorbed water, decomposition of the doped groups from the polymer chains in the interval of

200–330 °C and degradation of polymer backbone in the range of 330–800 °C [33]. The TGA thermograms of the s-PANINa and nanohybrid are similar, but the one-step degradation profile is observed for hybrid, indicating the interaction between the polymer matrix and the functionalized graphene sheets increased thermal stability of the hybrid [34].

The formation of nanohybrid further confirmed by XRD measurement in Fig. 4. The XRD pattern of GO-BI exhibits two peaks that appear at 10.8° and 25.8°. The peak at 10.8° corresponds to the (001) plane with an interlayer distance of 8.18 Å, which is due to the presence of functional groups on the graphene sheets. A (002) peak at 25.8° indicates that restacking of the graphene due to functionalization process [35]. For q-graphene, the (001) peak of the larger interlayer distance disappeared completely and only the abroad (002) peak at 26°, which corresponds to an interlayer distance of 8.18 Å are observed. These results suggest that the stacking of the graphene sheets was due to the van der Waals force interaction and linked the functional groups on the edges of graphene [22, 36]. Additionally, the broad peak with weak intensity can be explained by the electrostatic repulsion between the quaternary groups on the edges of graphene sheets and thus exhibits a high degree of exfoliated to few layers [37]. s-PANINa exhibits a typical semi-crystalline pattern [38], which improves the crystallinity of nanohybrid significantly. The XRD of hybrid presents new sharp and crystalline peaks indicating the existence of a new crystal structure

Table 1 Electrical conductivities of the different samples

Sample	q-graphene	s-PANINa	Nanohybrid
σ_e (S cm^{-1})	10.8	–	1000

[39]. However, the typical peak of q-graphene and s-PANINa completely disappears in nanohybrid, which demonstrates that the strengthened stacking along the specific direction between the functional groups of the q-graphene and the s-PANINa induces the crystallization of nanohybrid. Increasing in the crystalline character would affect the electrical properties of nanohybrid, which is significant for the capacitor application [16, 40].

The above discussion indicates that nanohybrid considerably should show better electrical conductivity comparison to s-PANINa and q-graphene. The electrical conductivity of the s-PANINa, q-graphene and nanohybrid is determined by a four-probe method, and the data are collected in Table 1. The q-graphene exhibits a conductivity of 10.8 S cm^{-1}. With addition insulating salts of the s-PANINa polymer to the q-graphene, the conductivity has increased to 1000 S cm^{-1}. Nanohybrid is exhibiting higher electrical conductivity owing to the formation of a π-conjugated structure between the s-PANINa and graphene with electrostatic interaction, which causes the more compact packing of the quinoid ring PANI chains on graphene surface, resulting in enhance in the electrical conductivity and degree of crystallinity [16, 41].

X-ray photoelectron spectroscopy (XPS) analysis is used to investigate the elemental compositions and the surface chemistry of the nanohybrid, the overall XPS spectrum of nanohybrid, as shown in Fig. 5a, revealed that nanohybrid is consisted of elemental C, N, O and S. The weak N1 s and S2p peaks in the XPS spectrum also confirm the s-PANINa surrounded by q-graphene sheets [42]. The high-resolution XPS spectrum of C1 s peaks centered at 284.8, 285.4, 286.5, 286.5, 288.3 and 291.7 eV, corresponding to carbon species of C–C, C–N, C–O, C=O and π–π*, respectively [43] (Fig. 5b). The strong π–π* conjugated system in nanohybrid demonstrates that the electron transfer facilitating between q-graphene and s-PANINa [44], and improving the electrochemical performance, which agreed well with the Raman analysis results, evidencing the outstanding conductivity of nanohybrid.
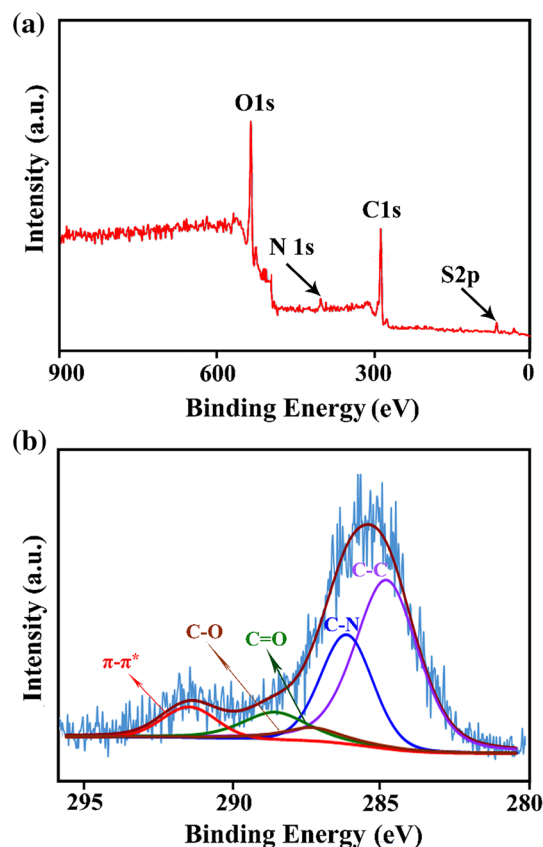

Figure 5 a Survey XPS spectrum of nanohybrid. **b** XPS data for C1 s region of nanohybrid.

Electrochemical behavior of the nanohybrid

Figure 6a compares the voltammograms of q-graphene, PANI and s-PANINa/q-graphene nanohybrid at the scan rate of 50 mV s^{-1} in the potential range of 0.0 to +0.8 V in 1.0 M of H$_2$SO$_4$. As can be seen, the shape of the cyclic voltammogram of PANI is different from an ideal rectangular shape, while nanohybrid exhibited a rectangular shape cyclic voltammogram with larger integrated area in comparison with PANI and q-graphene. The specific capacitances (C_s) (from cyclic voltammograms) were calculated according to the following equation [45]:

$$C_s = \frac{\int I dV}{2 \times m \times v \times \Delta V} \tag{1}$$

where $\int I dV$ is the integrated area of the CV curve, m (g) is the mass of the active material and ΔV (V) is the width of the potential window and v (V s^{-1}) is the potential scan rate. The results show that the specific capacitance of nanohybrid (570 F g^{-1}) is higher than for PANI (421 F g^{-1}) and for q-graphene (111 F g^{-1}). These results can be ascribed to the combination of

(A)

(B)
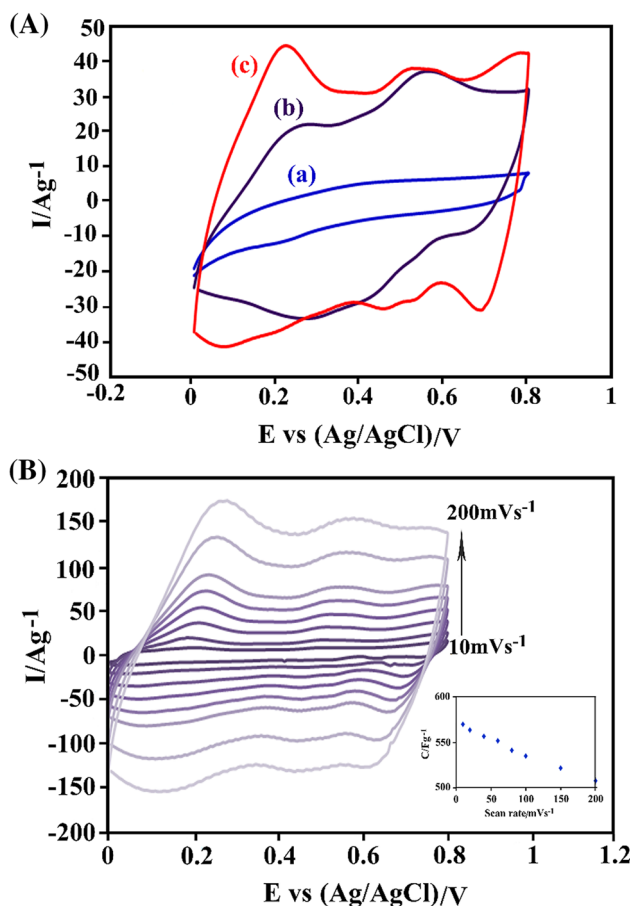
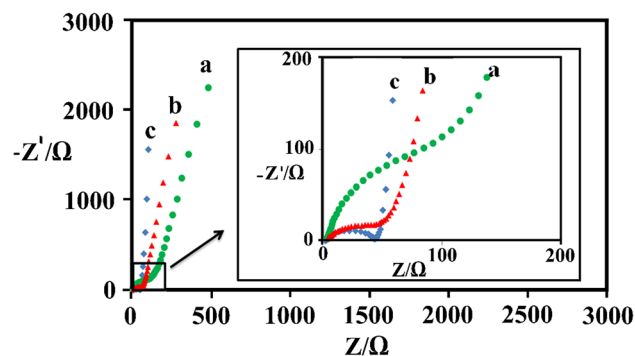**Figure 6** **a** Cyclic voltammograms of *a* graphene, *b* PANI and *c* s-PANINa/q-graphene at a scan rate of 50 mV s^{-1}; **b** effect of different scan rates on s-PANINa/q-graphene in 0.5 mol L. *Insets* of B: Variation of the specific capacitance versus scan rates.

Figure 7 Nyquist plots of *a* graphene, *b* PANI and *c* s-PANINa/q-graphene in a frequency range of 100 kHz–10 mHz under open-circuit condition with a potential perturbation of 10 mV.

charge storage properties of PANI and superior properties of q-graphene including high conductivity and high surface area.

Cyclic voltammograms of the nanohybrid in 1.0 M of H$_2$SO$_4$ were recorded at different scan rates (Fig. 6b). As can be seen, only a minor decrease was observed in the specific capacitances from the scan rate of 10–200 mv s^{-1} (20 times higher). This high-rate capability can be attributed to the high surface area of graphene which increases the number of active sites for polyaniline deposition and subsequently facilitating the charge and ion transport between nanohybrid and electrolyte [46].

Electrochemical impedance spectroscopy technique (EIS) has also been employed to understand the difference in the electrochemical behavior of s-PANINa/q-graphene nanohybrid compared with q-graphene and PANI. EIS of different electrodes are

shown in Fig. 7 the Nyquist form of impedance for the three electrodes all include a semicircle at high-frequency region and an approximately straight line at low-frequency end. The semicircle represents charge transfer resistance (Rct) at electrode/electrolyte interface. The lower Rct of the nanohybrid electrode (inset of Fig. 7) relative to q-graphene and PANI electrode reflects a more rapid redox rate at electrode/electrolyte interface. Also, as can be seen in Fig. 7, at low frequency, the nanohybrid electrode exhibited a more vertical line than q-graphene and PANI, which corresponded to a more ideal capacitor and a shorter ion diffusion path length of ions in the electrode material, which should facilitate the efficient access of electrolyte ions to the surfaces of s-PANINa/q-graphene nanohybrid.

For better comparison, CD curves of q-graphene, PANI and nanohybrid were also recorded in 1.0 M of H$_2$SO$_4$ at the current density of 2.0 A g^{-1} (Fig. 8a). All the CD curves show the ideal triangular shape with linear voltage change during charge and discharge steps. As can be seen, there is no IR drop in discharge curve of q-graphene, whereas PANI and nanohybrid exhibited an IR drop of about 70 and 30 mV at the beginning of discharging steps, respectively. Generally, IR drop at the turning point of CD curves is originated from internal resistance of electrode/active materials and electrolyte potential drop [47]; therefore, the negligible IR drop (30 mV) of nanohybrid can be attributed to the incorporation of highly conductive q-graphene to the PANI matrix and consequently the reduction in nanohybrid internal resistance. The specific capacitance of the electrode materials was calculated using the following equation [48]:
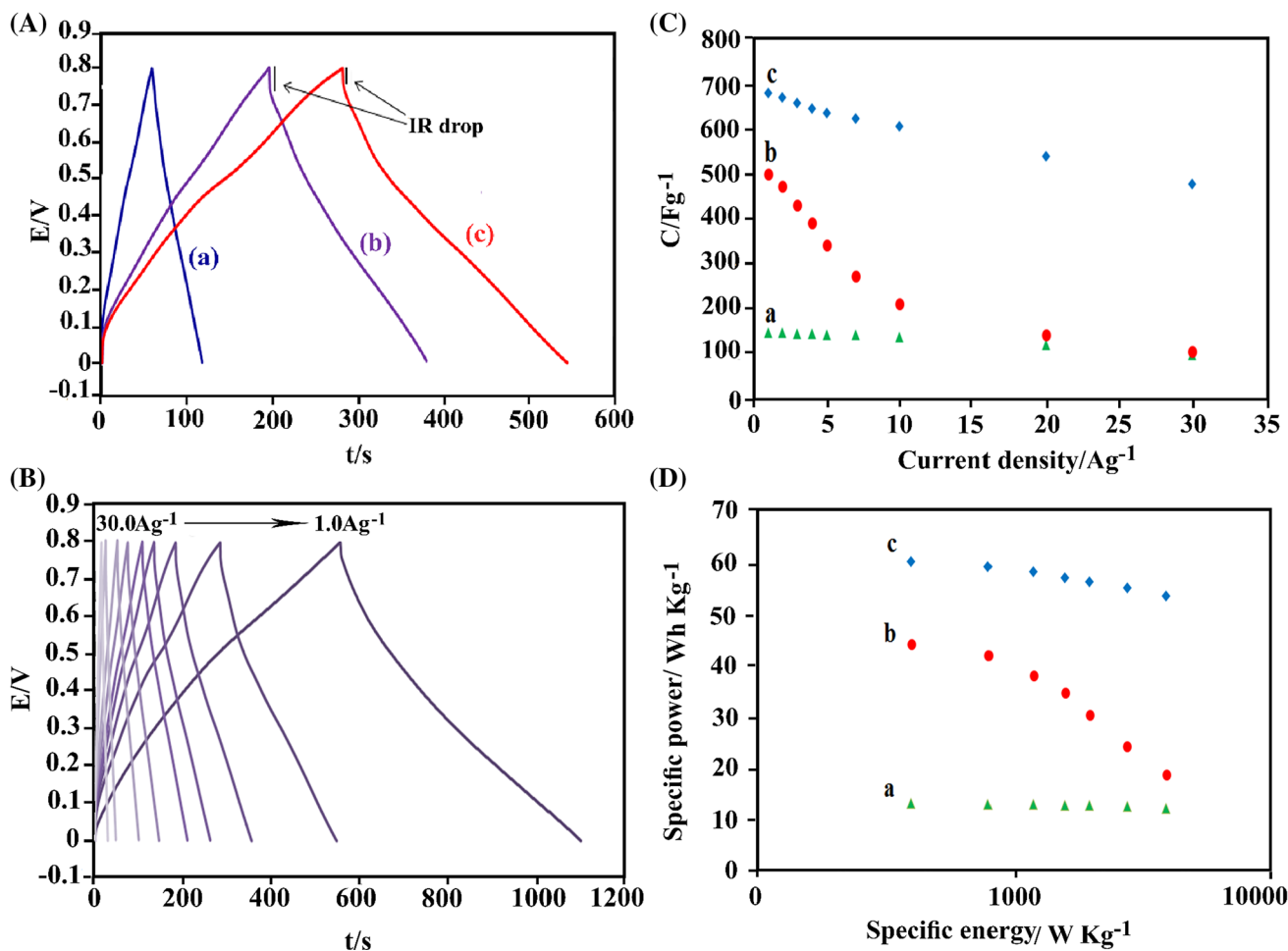
Figure 8 **a** CD tests of q-graphene, PANI and s-PANINa/q-graphene at a current density of 2.0 A g⁻¹; **b** effect of different current densities on capacitance properties of s-PANINa/q-graphene; **c** variation of the specific capacitance versus the current density for q-graphene, PANI and s-PANINa/q-graphene; **d** Ragone plots of q-graphene, PANI and s-PANINa/q-graphene at different current densities (1.0–30.0 A g⁻¹).

$$\text{Specific capacitance} = I.t/\Delta V.m \quad (4)$$

where I (A) and t (s) are the discharge current and time, respectively, ΔV (V) is the potential range, and m (g) is the mass loading of the active materials. In agreement with the CVs results, nanohybrid discharge curve exhibited higher specific capacitance (672 F g⁻¹) in comparison with PANI (475 F g⁻¹) and q-graphene (146 F g⁻¹) which indicates the crucial role of q-graphene in improvement in electrochemical performance of the PANI [46].

For further evaluation of nanohybrid as an electrode material for supercapacitors application, CD curves at different current densities were recorded in 1.0 M of H_2SO_4 (Fig. 8b). The plot of the specific capacitance versus current density (Fig. 8c) revealed

that PANI lost 78% of its capacitance when the discharge current density increased from 1.0 to 30.0 A g⁻¹, while nanohybrid retained 70% of its capacitance in the same condition. These results confirmed the good rate capability of the nanohybrid as a result of the combination of superior redox properties of PANI and attractive physicochemical properties of graphene such as high surface area, excellent electrical conductivity and good stability.

As two important parameters in supercapacitor electrode material specification, the specific power (SP, W kg⁻¹) and the specific energy (SE, W h kg⁻¹) were calculated from CD using the following relationships [49]:
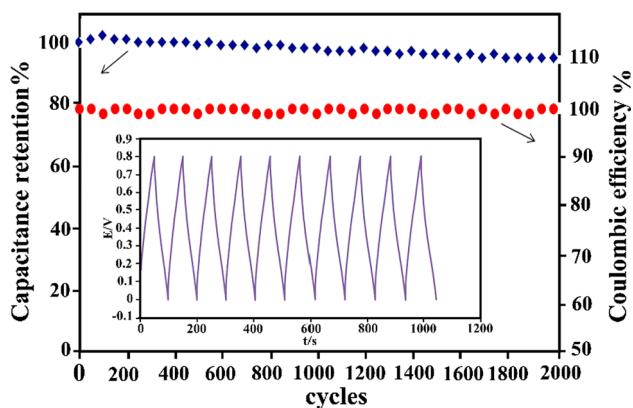
Figure 9 Capacitance retention and coulombic efficiency of s-PANINa/q-graphene in 1.0 mol. L^{-1} of H_2SO_4 at a current density of 10.0 A g^{-1} during 2000 cycles. *Inset* first 10 cycles.

$$SP = \frac{I\Delta V}{2m} \quad (5)$$

$$SE = 0.5\frac{C_s\Delta V^2}{3.6} \quad (6)$$

where I (A), ΔV (V) and m (g) are the discharge current, operating potential window and mass loading of the active materials in electrode, respectively. The overall operational characteristics of the q-graphene, PANI and nanohybrid electrode materials were demonstrated using the Ragone plot (Fig. 8d). The results show that nanohybrid presented higher specific energy in comparison with q-graphene and PANI at the same specific power which can be attributed to the excellent rate capability and high specific capacitance of nanohybrid. The maximum power density of 4000 W kg^{-1} at energy density of 54 W h kg^{-1} and in discharge current of 10.0 A g^{-1} was achieved for nanohybrid in 1.0 M of H_2SO_4 (Table S1).

Cycling stability of the electrode materials

The cycling stability and coulombic efficiency of nanohybrid were investigated in 1.0 M of H_2SO_4 at a current density of 10.0 A g^{-1} using CD test (Fig. 9). The results revealed that the proposed electrode material retains 95% of its original capacitance after 2000 cycles with coulombic efficiency of 100%. The high cyclic stability and excellent coulombic efficiency of the proposed electrode material can be ascribed to the negligible degradation of electrode matrix during charge/discharge process. Performance comparison of different graphene/PANI

Table 2 Specific capacitance, specific energy and specific power of s-PANINa/q-graphene at various current densities

current density (A g^{-1})	capacitance (F g^{-1})	specific energy (W h kg^{-1})	specific power (W kg^{-1})
1.0	682	60.6	400
2.0	672	59.7	800
3.0	660	58.7	1200
4.0	647	57.5	1600
5.0	638	56.7	2000
7.0	625	55.6	2800
10.0	607	54.0	4000

nanostructure-based electrodes for supercapacitor application [18, 26, 46, 50, 51] versus our proposed electrode material is given in Table 2. As can be seen, capacitance and long-term stability of the proposed electrode material is superior or at least comparable to those recently obtained by other works.

Conclusion

In this work, a new approach is introduced for synthesis of graphene/PANI nanohybrid based on electrostatic interaction of positively charged graphene nanosheets and negatively charged functionalized polyaniline. Utilizing this nanohybrid, a supercapacitor with a maximum capacitance of 682 F g^{-1} at a current density of 1.0 A g^{-1} and 90.0% retention of the initial specific capacitance (from current density of 1.0–10 A g^{-1}) has been achieved. The proposed nanohybrid also owns an excellent stability (less than 5% drop after 2000 cycles) with about 100% of coulombic efficiency. The reinforcement and synergetic effect between polyaniline and graphene leads to superior electrochemical properties, which makes the proposed nanohybrid, a promising candidate for electrode material in energy storage devices.

Acknowledgements

References

[1] Rahman AH, Majid MS, Rezaee Jordehi A, Chin Kim G, Hassan MY, Fadhl OS (2015) Operation and control strategies of integrated distributed energy resources: a review. Renew Sustain Energy Rev 51:1412–1420

[2] Wang G, Zhang L, Zhang J (2012) A review of electrode materials for electrochemical supercapacitors. Chem Soc Rev 41(2):797–828

[3] Zuliani JE, Caguiat JN, Kirk DW, Jia CQ (2015) Considerations for consistent characterization of electrochemical double-layer capacitor performance. J Power Sources 290:136–143

[4] Yang Y, Ren S, Ma S, Hao C, Ji M (2015) Hollow tin dioxide microspheres with multilayered nanocrystalline shells for pseudocapacitor. Electrochim Acta 155:437–446

[5] Mu B, Zhang W, Xu W, Wang A (2015) Hollowed-out tubular carbon@ MnO2 hybrid composites with controlled morphology derived from kapok fibers for supercapacitor electrode materials. Electrochim Acta 178:709–720

[6] Wang J, Ma R, Zhou Z, Liu G, Liu Q (2015) Magnesiothermic synthesis of sulfur-doped graphene as an efficient metal-free electrocatalyst for oxygen reduction. Sci Rep 5:9304

[7] Li M, Cheng JP, Liu F, Zhang XB (2015) In situ growth of nickel-cobalt oxyhydroxide/oxide on carbon nanotubes for high performance supercapacitors. Electrochim Acta 178: 439–446

[8] Su Y, Zhitomirsky I (2015) Asymmetric electrochemical supercapacitor, based on polypyrrole coated carbon nanotube electrodes. Appl Energy 153:48–55

[9] Huang K-J, Wang L, Zhang J-Z, Xing K (2015) Synthesis of molybdenum disulfide/carbon aerogel composites for supercapacitors electrode material application. J Electroanal Chem 752:33–40

[10] Shao Z, Li H, Li M, Li C, Qu C, Yang B (2015) Fabrication of polyaniline nanowire/TiO2 nanotube array electrode for supercapacitors. Energy 87:578–585

[11] Snook GA, Kao P, Best AS (2011) Conducting-polymer-based supercapacitor devices and electrodes. J Power Sources 196(1):1–12

[12] Shen K, Ran F, Zhang X, Liu C, Wang N, Niu X, Liu Y, Zhang D, Kong L, Kang L, Chen S (2015) Supercapacitor electrodes based on nano-polyaniline deposited on hollow carbon spheres derived from cross-linked co-polymers. Synth Met 209:369–376

[13] Zhang X, Zhang H, Li C, Wang K, Sun X, Ma Y (2014) Recent advances in porous graphene materials for supercapacitor applications. RSC Adv 4(86):45862–45884

[14] Biswas S, Drzal LT (2010) Multilayered nanoarchitecture of graphene nanosheets and polypyrrole nanowires for high performance supercapacitor electrodes. Chem Mater 22(20):5667–5671

[15] Sun D, Jin L, Chen Y, Zhang JR, Zhu JJ (2013) Microwave-assisted in situ synthesis of graphene/PEDOT hybrid and its application in supercapacitors. ChemPlusChem 78(3):227–234

[16] Kim M, Lee C, Jang J (2014) Fabrication of highly flexible, scalable, and high-performance supercapacitors using polyaniline/reduced graphene oxide film with enhanced electrical conductivity and crystallinity. Adv Funct Mater 24(17):2489–2499

[17] Song B, Li L, Lin Z, Wu Z-K, K-s Moon, Wong C-P (2015) Water-dispersible graphene/polyaniline composites for flexible micro-supercapacitors with high energy densities. Nano Energy 16:470–478

[18] Cao H, Zhou X, Zhang Y, Chen L, Liu Z (2013) Microspherical polyaniline/graphene nanocomposites for high performance supercapacitors. J Power Sources 243:715–720

[19] Tamai H, Hakoda M, Shiono T, Yasuda H (2007) Preparation of polyaniline coated activated carbon and their electrode performance for supercapacitor. J Mater Sci 42(4):1293–1298. doi:10.1007/s10853-006-1059-7

[20] Zhao HB, Yang J, Lin TT, Lü QF, Chen G (2015) Nanocomposites of sulfonic polyaniline nanoarrays on graphene nanosheets with an improved supercapacitor performance. Chem A Eur J 21(2):682–690

[21] Jianhua L, Junwei A, Yecheng Z, Yuxiao M, Mengliu L, Mei Y, Songmei L (2012) Preparation of an amide group-connected graphene-polyaniline nanofiber hybrid and its application in supercapacitors. ACS Appl Mater Interfaces 4(6):2870–2876

[22] Zuo Z, Li W, Manthiram A (2013) N-heterocycles tethered graphene as efficient metal-free catalysts for an oxygen reduction reaction in fuel cells. J Mater Chem A 1(35):10166–10172

[23] Luo J, Chen Y, Ma Q, Liu R, Liu X (2014) Layer-by-layer assembled ionic-liquid functionalized graphene–polyaniline nanocomposite with enhanced electrochemical sensing properties. J Mater Chem C 2(24):4818–4827

[24] Dimiev A, Kosynkin DV, Alemany LB, Chaguine P, Tour JM (2012) Pristine graphite oxide. J Am Chem Soc 134(5):2815–2822

[25] Ansari MO, Khan MM, Ansari SA, Amal I, Lee J, Cho MH (2014) pTSA doped conducting graphene/polyaniline nanocomposite fibers: thermoelectric behavior and electrode analysis. Chem Eng J 242:155–161

[26] Fan T, Tong S, Zeng W, Niu Q, Liu Y, Kao C-Y, Liu J, Huang W, Min Y, Epstein AJ (2015) Self-assembling sulfonated graphene/polyaniline nanocomposite paper for high performance supercapacitor. Synth Met 199:79–86

[27] Ai W, Zhou W, Du Z, Du Y, Zhang H, Jia X, Xie L, Yi M, Yu T, Huang W (2012) Benzoxazole and benzimidazole heterocycle-grafted graphene for high-performance supercapacitor electrodes. J Mater Chem 22(44):23439–23446

[28] Chen S-A, Hwang G-W (1996) Structure characterization of self-acid-doped sulfonic acid ring-substituted polyaniline in its aqueous solutions and as solid film. Macromolecules 29(11):3950–3955

[29] Agrawalla RK, Paul S, Sahoo PK, Chakraborty AK, Mitra AK (2015) A facile synthesis of a novel three phase nanocomposite: Single wall carbon nanotube/silver nanohybrid fibers embedded in sulfonated polyaniline. J Appl Polymer Sci 132(12):41692

[30] Ferrari AC (2007) Raman spectroscopy of graphene and graphite: disorder, electron–phonon coupling, doping and nonadiabatic effects. Solid state Commun 143(1–2):47–57

[31] Liang B, Qin Z, Li T, Dou Z, Zeng F, Cai Y, Zhu M, Zhou Z (2015) Poly(aniline-co-pyrrole) on the surface of reduced graphene oxide as high-performance electrode materials for supercapacitors. Electrochimica Acta 177:335–342

[32] Xu T, Xin M, Li M, Huang H, Zhou S, Liu J (2011) Synthesis, characterization, and antibacterial activity of N, O-quaternary ammonium chitosan. Carbohydr Res 346(15): 2445–2450

[33] Xu J, Yao P, Li X, He F (2008) Synthesis and characterization of water-soluble and conducting sulfonated polyaniline/para-phenylenediamine-functionalized multi-walled carbon nanotubes nano-composite. Mater Sci Eng B 151(3):210–219

[34] Li X, Yu Y, Meng Y (2013) Novel quaternized poly(arylene ether sulfone)/Nano-ZrO(2) composite anion exchange membranes for alkaline fuel cells. ACS Appl Mater Interfaces 5(4):1414–1422

[35] Ai W, Liu J-Q, Du Z-Z, Liu X-X, Shang J-Z, Yi M-D, Xie L-H, Zhang J-J, Lin H-F, Yu T (2013) One-pot, aqueous-phase synthesis of graphene oxide functionalized with heterocyclic groups to give increased solubility in organic solvents. RSC Adv 3(1):45–49

[36] Gao Z, Yang W, Wang J, Yan H, Yao Y, Ma J, Wang B, Zhang M, Liu L (2013) Electrochemical synthesis of layer-by-layer reduced graphene oxide sheets/polyaniline nanofibers composite and its electrochemical performance. Electrochim Acta 91:185–194

[37] Bae S-Y, Jeon I-Y, Yang J, Park N, Shin HS, Park S, Ruoff RS, Dai L, Baek J-B (2011) Large-area graphene films by simple solution casting of edge-selectively functionalized graphite. ACS Nano 5(6):4974–4980

[38] Bhadra S, Kim NH, Lee JH (2010) Synthesis of water soluble sulfonated polyaniline and determination of crystal structure. J Appl Polym Sci 117(4):2025–2035

[39] Li X, Yu Y, Meng Y (2013) Novel quaternized poly (arylene ether sulfone)/nano-ZrO2 composite anion exchange membranes for alkaline fuel cells. ACS Appl Mater Interfaces 5(4):1414–1422

[40] Nguyen VH, Tang L, Shim J-J (2013) Electrochemical property of graphene oxide/polyaniline composite prepared by in situ interfacial polymerization. Colloid Polym Sci 291(9):2237–2243

[41] Gedela VR, Srikanth VVSS (2014) Electrochemically active polyaniline nanofibers (PANi NFs) coated graphene nanosheets/PANi NFs composite coated on different flexible substrates. Synth Met 193:71–76

[42] Chen Y, Lu S, Wu X, Liu J (2015) Flexible carbon nanotubes-graphene/sulfur composite film: free-standing cathode for high-performance lithium/sulfur batteries. J Phys Chem C 119(19):10288–10294

[43] Zhao HB, Yang J, Lin TT, Lu QF, Chen G (2015) Nanocomposites of sulfonic polyaniline nanoarrays on graphene nanosheets with an improved supercapacitor performance. Chemistry 21(2):682–690

[44] Luo Y, Kong D, Jia Y, Luo J, Lu Y, Zhang D, Qiu K, Li CM, Yu T (2013) Self-assembled graphene@ PANI nanoworm composites with enhanced supercapacitor performance. Rsc Adv 3(17):5851–5859

[45] Ensafi AA, Ahmadi N, Rezaei B (2015) Electrochemical preparation of CuBi2O4 nanoparticles on nanoporous stainless steel as a binder-free supercapacitor electrode. J Alloy Compd 652:39–47

[46] Sun H, She P, Xu K, Shang Y, Yin S, Liu Z (2015) A self-standing nanocomposite foam of polyaniline@reduced graphene oxide for flexible super-capacitors. Synth Met 209:68–73

[47] Hao J, Liao Y, Zhong Y, Shu D, He C, Guo S, Huang Y, Zhong J, Hu L (2015) Three-dimensional graphene layers prepared by a gas-foaming method for supercapacitor applications. Carbon 94:879–887

[48] Zhang X-Y, Han L-Q, Sun S, Wang C-Y, Chen M-M (2015) MnO2/C composite electrodes free of conductive enhancer for supercapacitors. J Alloy Compd 653:539–545

[49] Ghasemi S, Ojani R, Ausi S (2014) Bipotential deposition of nickel–cobalt hexacyanoferrate nanostructure on graphene coated stainless steel for supercapacitors. Int J Hydrogen Energy 39(27):14918–14926

[50] Liu H, Zhang W, Song H, Chen X, Zhou J, Ma Z (2014) Tremella-like graphene/polyaniline spherical electrode material for supercapacitors. Electrochim Acta 146:511–517

[51] Wang S, Ma L, Gan M, Fu S, Dai W, Zhou T, Sun X, Wang H, Wang H (2015) Free-standing 3D graphene/polyaniline composite film electrodes for high-performance supercapacitors. J Power Sources 299:347–355